A Varactor Loaded Tunable Dual-band Left-Handed Metamaterial

Si Li [1], Wenhua Yu [3], Atef Z. Elsherbeni [4], Wenxing Li [2], and Yunlong Mao [1]

[1] School of Electronic Information
Jiangsu University of Science and Technology, Zhenjiang, Jiangsu, 212003, China
lisi0511@just.edu.cn, maoyunlong0511@just.edu.cn

[2] College of Information and Communication
Harbin Engineering University, Harbin, Heilongjiang, 150001, China
liwenxing@hrbeu.edu.cn

[3] 2COMU, INC. Fairfax, VA 22030, USA
Wenyu@2comu.com

[4] Electrical Engineering Department
Colorado School of Mines, Golden, CO, 80401, USA
aelsherb@mines.edu

Abstract ─ In this paper, we proposed a tunable dual-band left-handed metamaterial (LHM). This dual-band LHM can be regarded as a combination of double-slits split ring resonators (DSSRRs) and rotated 'H-shape' structure loaded with varactors. The 'H-shape' structure functions like arrayed metallic wires, and is only capable of extracting negative permittivity, but with proper loaded capacitors, it can also extract negative permeability. According to the numerical analysis, such character is closely related to the mutual coupling coefficient. We analyzed both the DSSRRs and the 'H-shape' structure through equivalent circuits and simulations, respectively. Later the composed LHM loaded with varactors is also simulated. Dual-band left handed (LH) property can be observed from the retrieved effective parameters, of whom one LH band is stable and wide, approximately from 2GHz to 2.1GHz, while the other one is relatively narrow, shifting from 1.14GHz to 2.36GHz dynamically. Compared to other work where only multi-band technology or tunable method is applied, the combination of both the methods greatly extended the functioning bandwidth.

Index Terms ─ Dual-band, LHM, Tunable, Varactor-loaded.

I. INTRODUCTION

Metamaterials (MTMs) have aroused great attention since Pendry introduced periodically located metallic wires to achieve negative permittivity in 1996 [1]. Later, his team proposed spilt ring resonators (SRRs) to get negative permeability [2]. In [3,4], the authors composed SRRs and metallic wires together to get negative permittivity and permeability at the same frequency range. These kind of MTMs are also referred to as left-handed metamaterials (LHMs). However, even after so many years' development, the bandwidth limitation of MTMs remains a great challenge. There are two potential ways to cross this limitation.

Some researchers focused their studies on multi-band MTMs. The first kind of multi-band MTMs are based on well-designed metallic patterns, such as the 'S-shaped' [3], the 'H-shaped' [4] and the 'Z-shaped' [5] MTMs. An advanced well-designed metallic pattern mode is fractal shapes, such as the nested 'U-shaped' and the 'tree-shaped' [6] MTMs. Another kind of multi-band MTMs are implemented with a combination of different single-band MTM units. In [7], similar patterns are printed on different substrates, while in [8], SRRs with different opening directions are printed on 3 layers substrates.

Some researchers focused on the studies on tunable MTMs. There are multiple methods to implement tunable characteristics, such as loading varactors [9-17], applying ferrite slabs [18-21] or liquid crystal [22,23], and mechanically changing the structures [24-28]. Among these methods, varactor loaded tunability is the most applicable.

In this paper, we propose a tunable dual-band LHM to achieve a dynamical wideband. The geometry of this MTM is the same as the single-band LHM that Xin and his team published in 'Nature Communications' [29], while the loaded diode is replaced with a varactor. This single-band LHM unit can be regarded as a combination

Submitted On: May 28, 2017
Accepted On: December 24, 2018

of double-slits split ring resonators (DSSRR) and a rotated 'H-shape' structure. The 'H-shape' structure acts as arrayed metallic wires that are only capable of providing negative permittivity, however, with proper loaded capacitors, it also exhibits negative permeability. In this paper, both the basic particles of the single-band LHM are analyzed with equivalent circuits and simulations. After that, we loaded varactor diodes, the SMV-1236 from Skyworks, to the LHM. Simulations are operated with linearly increased reversed voltage from 0V to 5V, and retrieve the S parameters through the 'S-parameter retrieval method' published in [30] to get the effective parameters.

II. MODEL AND EQUIVALENT CIRCUIT

The geometry of the single-band LHM proposed in [29] is displayed in Fig. 1, where a=27 mm, b=54 mm, c=4 mm, d=5 mm, e=6 mm, f=0.8 mm, g=2.5 mm, r1=9 mm, r2=12 mm. The metallic pattern is printed on a 1.27 mm-thick Rogers-6006 substrate whose relative permittivity is 6.15, and the thickness of the metallic wires is t=0.017 mm.

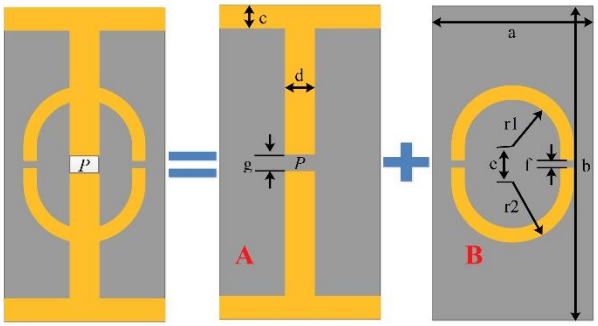

Fig. 1. Geometry illustration of the LHM proposed in [29]. It can be regarded as a combination of a rotated 'H-shape' (particle A) and a DSSRR (particle B).

Such structure can be regarded as a combination of rotated 'H-shape' metallic wires (particle A) and DSSRRs (particle B). In the discussed frequency regime [29], DSSRRs produce negative permeability while the rotated 'H-shaped' structure is responsible for negative permittivity.

A. Equivalent circuit analysis for particle A

In [31], the authors proposed a double-sided rotated 'H-shape' structure where the magnetic resonance is originated from the anti-paralleled currents in the wires with opposite signs accumulating at corresponding ends. Similarly, a proper capacitor loaded will also generate anti-paralleled currents on both ends.

According to the theoretical analysis of the split ring resonators (SRRs) proposed in [2,29], the magnetic resonance is motivated by the electromotive force around the circumference of the split rings. Considering an infinite array of such SRRs arranged in three orthogonal directions with a spatial period of *d*, and an incident magnetic field polarized along the y direction, that is, perpendicular to the SRRs, there would be electromotive force and induced current *I* along the rings, satisfying:

$$\begin{aligned} \mathrm{EMF} &= j\omega\pi r^2\mu_0 H_0 \\ &= RI + I/(-j\omega C) + (-j\omega L)I + j\omega FLI, \end{aligned} \quad (1)$$

where H_0 is the external magnetic field, *R*, *L*, and *C* are the parasitic resistance, the geometrical inductance, and the capacitance of each ring, respectively, and *FL* is the mutual inductance between different rings. With $L = \pi r^2\mu_0 / d$, and $F = \pi r^2 / d^2$, the current *I* is given as:

$$I = \frac{-j\omega\pi r^2\mu_0 H_0}{j\omega L[1-F] - R + \dfrac{1}{j\omega C}} = \frac{-dH_0}{\left(1 - F - \dfrac{1}{\omega^2 LC}\right) + \dfrac{Rj}{\omega L}}. \quad (2)$$

Based on the magnetic moment per unit volume, $M = \pi r^2 I / d^3$ and $\mu_{eff} = (B/\mu_0)/(B/\mu_0 - M)$, *B* is the corresponding external magnetic flux, then we can obtain the final effective permeability as following:

$$\mu_{eff} = 1 - \frac{F\left(1 - \dfrac{1}{\omega^2 LC}\right) - j\dfrac{R}{\omega L}}{\left(1 - \dfrac{1}{\omega^2 LC}\right)^2 + \dfrac{R^2}{(\omega L)^2}}. \quad (3)$$

From the analysis above, it is obvious that the effective permeability is completely irrelevant with the shape of the magnetic resonators, but closely related to the mutual coupling and self-properties of the structure.

The equivalent circuit for the rotated 'H-shape' wire with an embedded capacitor C_e is displayed in Fig. 2, where L_e is the equivalent inductance.

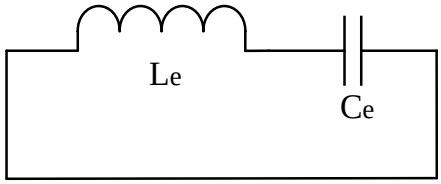

Fig. 2. Equivalent circuit of the rotated 'H-shape'.

The self-inductance of a strip line can be calculated using [32]:

$$L = 2\times10^{-4} l\left[\ln\left(\frac{l}{w+t}\right) + 1.193 + 0.2235\frac{w+t}{l}\right], \quad (4)$$

where *l* is the length of the strip line, *w* is the width, and *t* is the thickness. Assume a function 'Cal_induc(l,w,t)' to represent (4), then for particle A, equivalent inductance L_e can be approximated as:

$$L_e = cal\_indc(b/2, d, t), \quad (5)$$

which is 0.72 nH. Hence, the magnetic resonant frequency can be calculated as:

$$f_m = \frac{1}{2\pi\sqrt{L_e C_e}}. \quad (6)$$

We listed the corresponding resonant frequencies while C_e ranging from 7 Pf to 25 Pf with a step size of 3 Pf in Table 1. The resonant frequency is linearly shifting from higher frequencies to lower frequencies with the increase of C_e.

Table 1: Resonant frequencies with C_e ranging

C_e(pF)	7	10	13	16	19
f_m(GHz)	2.25	1.88	1.65	1.49	1.37

B. Equivalent circuit analysis for particle B

The equivalent circuit for the DSSRR is displayed in Fig. 3.

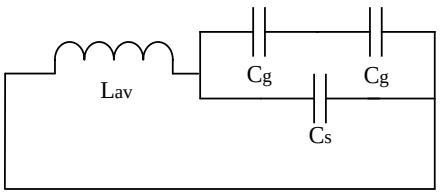

Fig. 3. Equivalent circuit for DSSRR.

The total equivalent capacitance of DSSRR is calculated as:

$$C_{total} = C_g/2 + C_s, \quad (7)$$

where C_g is the gap capacitance, and C_s is the surface capacitance.

According to the transmission line theory [32], for the coplanar strips on a substrate as illustrated in Fig. 4, the capacitance per unit length of the paralleled strip lines are calculated using:

$$C_{pul} = \varepsilon_0 \varepsilon_e F(k), \quad (8)$$

where ε_0 is the permittivity of free space, ε_e and the first kind elliptic integral related function *F(k)* are calculated as:

$$\varepsilon_e = 1 + (\varepsilon_r - 1) F(k)/2F(k1), \quad (9)$$

$$F(k) = \begin{cases} \frac{1}{\pi}\ln(2\frac{1+\sqrt{k'}}{1-\sqrt{k'}}), & 0 < k \le \frac{1}{\sqrt{2}} \\ \pi\ln(2\frac{1+\sqrt{k}}{1-\sqrt{k}})^{-1}, & \frac{1}{\sqrt{2}} < k \le 1 \end{cases}, \quad (10)$$

where $k=a/b$, $a=s/2$, $b=w+s/2$, $k' = \sqrt{1-k^2}$, and $k1 = \sinh(\pi a/2h)/\sinh(\pi b/2h)$.

In this example, with respect to the estimation method [33], *s = f*, and *w=r1 + (e-f)/2*; hence C_g can be calculated which is 0.142pf. The calculation for $C_s = C_{s1} + C_{s2}$ is approximated as [34]:

$$\begin{cases} C_{s1} = \frac{\varepsilon_0 (t + r2 - r1)}{\pi}\left(\log\frac{2(r1+r2)}{g} + e - f\right) \\ C_{s2} = \frac{\varepsilon_0 (\varepsilon_r - 1)(t + r2 - r1)}{2\pi}\left(\log\frac{2(r1+r2)}{g} + e - f\right) \end{cases}, \quad (11)$$

where C_{s1} is the surface capacitance through air, C_{s2} is the surface capacitance through the substrate, hence, C_s = 0.192pf. Then total capacitance Ct is 0.264pf.

The total equivalent inductance for the double slits SRR can also be approximated using (4), and it can also be approximated as:

$$L_{av} = cal\_indc(r2 - r1, \pi(r1+r2)/2 + e - f, t), \quad (12)$$

therefore, the resonant frequency for the double slits SRR can also be calculated using a similar equation as (6), which is 1.83GHz.

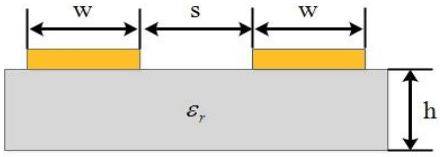

Fig. 4. Coplanar strips model.

III. SMULATIONS AND ANALYSIS

To verify the numerical analysis above, we ran simulations for particle A and B, respectively. After that, we introduced a varactor diode, SMV-1236 from Skyworks, and embedded it to the composed LHM. All the simulations are operated with HFSS software.

A. Simulation for particle A

For particle A, we ran the simulations with the embedded capacitance C_e varying from 7 pF to 19 pF linearly with a step size of 3 pF for the sake of simplify the analysis. Then we applied 'S parameters retrieval method' to get the effective parameters from simulated S parameters. The real part of the retrieved effective permittivity and permeability are displayed in Figs. 5 (a) and (b).

It is seen that particle A is capable of providing negative permittivity, and this property is quite similar to that of arrayed metallic wires. When C_e is 7 pF, 10 pF, and 13 pF, the effective permeability is also negative. For other values of C_e, there are also significant resonances. Compared to the resonant frequencies listed in Table 1, the simulated results match well with the numerical analysis. Hence, particle A can also be regarded as a single-band LHM with proper loaded capacitors, and it is tunable with the change of the capacitance.

B. Simulation for particle B

The simulated S parameters and the retrieved effective parameters are displayed in Figs. 6 (a) and (b).

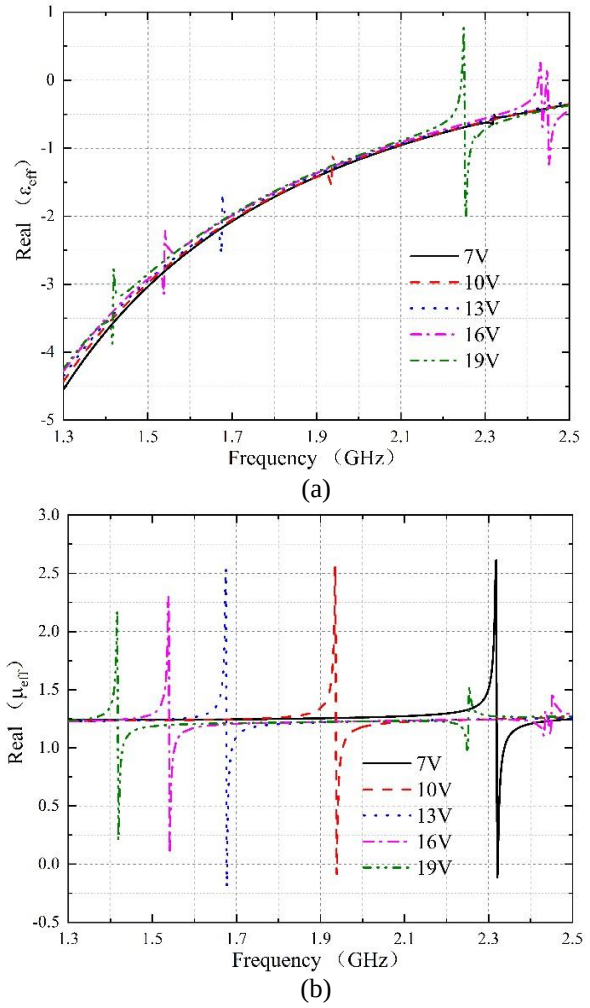

Fig. 5. Retrieved effective (a) permittivity and (b) permeability of the rotated 'H-shape' with the embedded capacitance varying from 7pF to 19pF.

Negative permittivity can be observed at a frequency range from 1.854GHz to 1.96GHz. The simulated results also match well with the numerical analysis.

C. Varactor-loaded LHM

In the previous sections, the tunability is discussed with a series of linearly changed capacitance for simplicity. However, in applications, tunable capacitors are usually achieved with varactor diodes. The proper varactor chosen is SMV1236 from Skyworks, and its spice model is displayed in Fig. 7 [35].

The capacitance 'CT' for this diode with the change of reversed voltage 'VR' is also listed in Table 2.

Simulations for the LHM with varactors loaded were operated and the S parameters are displayed in Fig. 8, the real part of the retrieved effective parameters are displayed in Figs. 9 (a), (b) and (c), with the reversed voltage ranging from 0V to 5V.

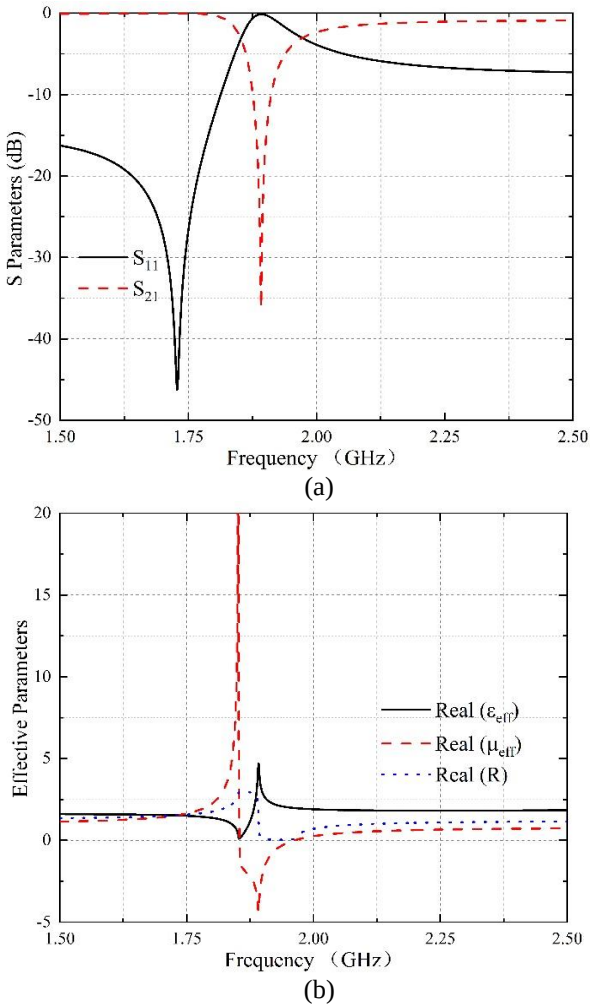

Fig. 6. (a) Simulated S parameters of DSSRR, and (b) the corresponding real part of the retrieved effective permittivity (Real(ε)), permeability (Real(μ)) and the refractive index (Real(R)).

Table 2: Total capacitance CT(pF) of the diodes varying with the reversed voltage VR(V)

VR	0	0.5	1	1.5	2	2.5
CT	26.75	20.61	17.02	14.38	12.29	10.56
VR	3	3.5	4	4.5	5	
CT	9.16	8.04	7.19	6.53	6.01	

In Fig. 8, there are 3 resonant frequencies despite the change of the reversed voltage, of whom two are only slightly shifted, while the other one is moving from lower frequencies to higher frequencies with the reversed voltage increases. Additionally, the bandwidth of the third resonance is only comparable with the stable

two ones when they are close.

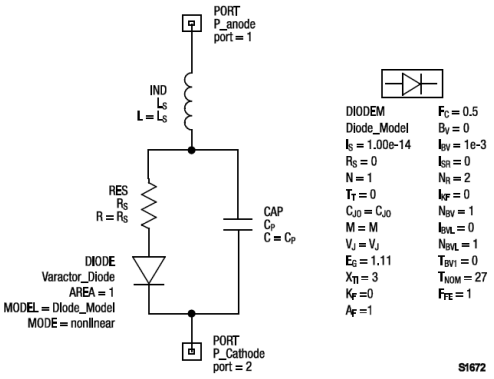

Fig. 7. The spice model of SMV1236.

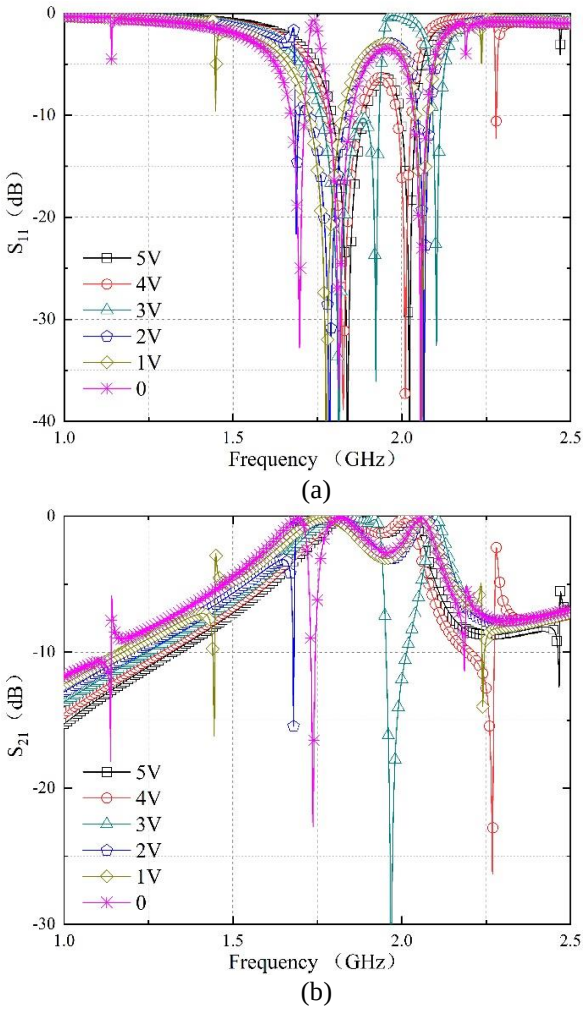

Fig. 8. Simulated (a) S_{11} and (b) S_{21} with reversed voltage ranging from 0V to 5V.

In Fig. 9 (a), permittivity is negative in the discussed frequency range only except for a narrow band approximately from 1.7GHz to 1.9GHz. In Fig. 9 (b), permeability is negative at two different frequency range, of whom one is narrow while the other one is comparable wide. Additionally, with the increase of VR, one of the negative regime is moving from lower frequencies to higher frequencies, while the other one is only slightly changed. Besides, the resonant strength of the shifting resonance gets stronger as it is moving closer to the stable resonance, such as the strong resonance when the reversed voltage is 3V. The refractive index displayed in Fig. 9 (c) show a similar property, and it remains negative despite of the change of VR.

We also listed more detailed information about the double negative band with VR changing at a step of 0.5V in Table 3, where 'LH-1' and 'LH-2' refers to the two left handed negative bands, and 'BW' refers to the corresponding bandwidth. They all measured with 'GHz'. Obviously, 'LH-1' is stable, while 'LH-2' is changeable. Compared to the previous discussed particle A and B, it can be developed that 'LH-1' is closely related to the DSSRR, while 'LH-2' is closely related to the rotated 'H-shape' with embedded varactor.

In this table, for 'LH-2', when VR=2.5V, only permeability is negative, and when VR=5V, only permittivity is negative, hence, they are all marked with 'null' in the table. From the point of bandwidth, it is interesting to note that the bandwidth for 'LH-2' gets wider as the two LH bands getting closer.

From (3), the real part of permeability is closely related to the mutual coupling. Hence, when the resonant frequencies of the two particles are getting closer, the LH bandwidth originates from particle A is also getting wider.

Table 4 listed the relative bandwidth of some previous work where 'MB' refers to multi-band method, 'VL' refers to the varactor-loaded method, and 'BW' refers to the relative bandwidth. In our work, the 0.2GHz wide right-handed bandwidth is excluded in the calculation for relative bandwidth. Apparently, with the combination of multi-band and tunable technology, the LH bandwidth is greatly extended.

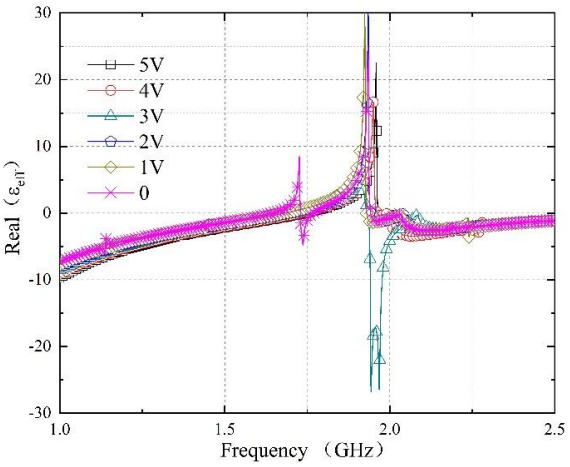

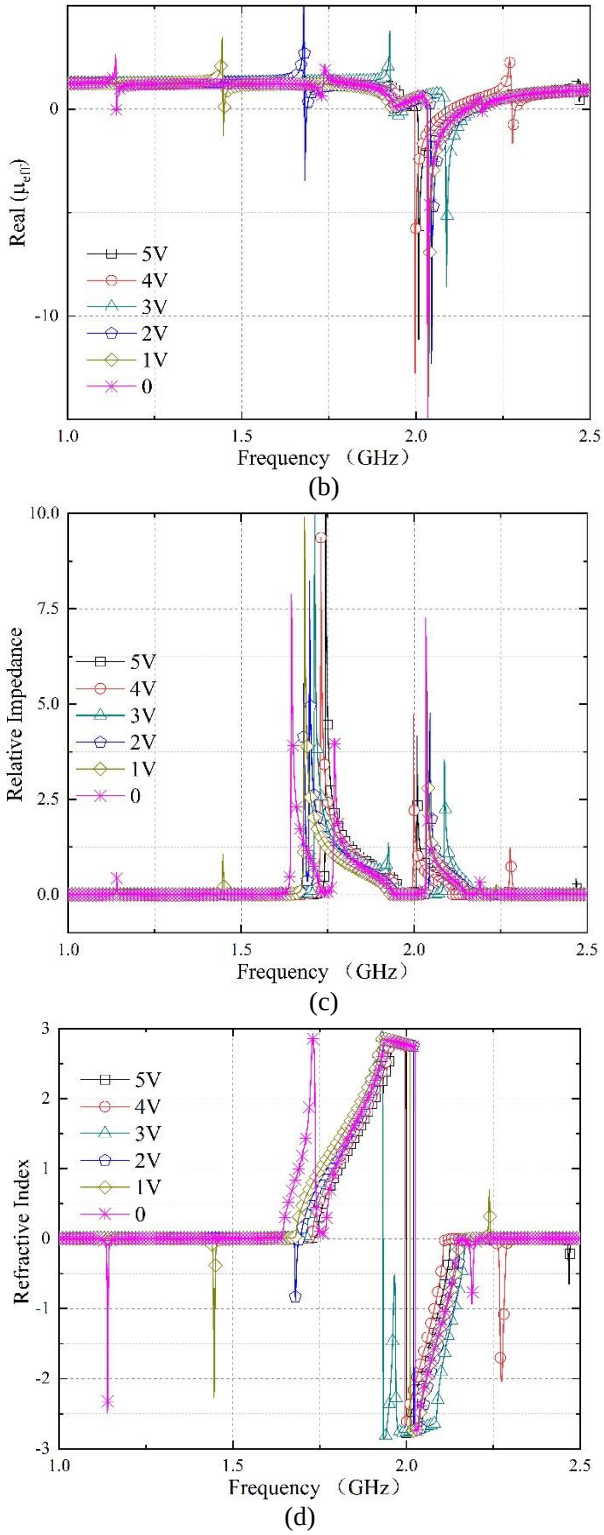

Fig. 9. The real part of the retrieved effective (a) permittivity, (b) permeability, (c) relative impedance, and (d) refractive index with the reversed voltage ranging from 0V to 5V.

Table 3: LH frequency range with VR changing

VR	LH-1	BW	LH-2	BW
0	2.032~2.144	0.112	1.142~1.14	0.002
0.5	2.034~2.15	0.116	1.311~1.313	0.002
1	2.034~2.151	0.116	1.446~1.450	0.004
1.5	2.039~2.155	0.116	1.568~1.573	0.005
2	2.041~2.156	0.115	1.680~1.688	0.008
2.5	2.054~2.161	0.107	null	null
3	2.084~2.167	0.083	1.933~1.964	0.031
3.5	1.975~2.060	0.085	2.161~2.202	0.041
4	1.995~2.107	0.112	2.275~2.287	0.012
4.5	2.003~2.123	0.12	2.363~2.368	0.005
5	2.003~2.125	0.122	null	null

Table 4: Relative bandwidth in some references using different methods

Ref	**Method**	**BW (%)**
[5]	MB	13.3
[6]	MB	25.3
[36]	MB	18.5
[9]	VL	27
[10]	VL	23
[11]	VL	38
This work	MB-VL	61.5

IV. CONCLUSION

In this paper, we proposed a varactor-loaded tunable dual-band LHM. The structure of this LHM without the varactor can be regarded as a combination of DSSRRs, that responsible for providing negative permeability, and rotated 'H-shape' structure that function as arrayed metallic wires providing negative permittivity. In our work, we analyzed both the basic particles with equivalent circuits and simulations and pointed out that the rotated 'H-shape' exhibits double negative properties with proper embedded capacitance. The loaded varactor is SMV-1236 from Skyworks. With the reversed voltage varying from 0V to 5V, there are two different frequency regimes with LHM properties, of whom one is wide and stable, approximately from 2GHz to 2.1GHz, while the other one is relatively narrow and is dynamically shifting from 1.14GHz to 2.34GHz except for frequencies between 1.7GHz to 1.9GHz. Additionally, when the two bands are close, the bandwidth of the wider one gets narrower, while the narrow one gets wider. Compared to other work where only multi-band technology or tunable method is applied, the combination of both the methods greatly extended the functioning bandwidth and can be of great use in areas such as radars and sensors.

REFERENCES

[1] J. B. Pendry, A. J. Holden, W. J. Stewart, and I. I. Youngs, "Extremely low frequency plasmons in metallic mesostructures," *Phys. Rev. Lett.*, vol. 76,

no. 25, pp. 4773-4776, June 17, 1996.

[2] J. B. Pendry, A. J. Holden, D. J. Robbins, and W. J. Stewart, "Magnetism from conductors and enhanced nonlinear phenomena," *IEEE Transactions on Microwave Theory and Techniques*, vol. 47, no. 11, pp. 2075-2084, 1999.

[3] H. Chen, et al., "Metamaterial exhibiting left-handed properties over multiple frequency bands," *Journal of Applied Physics*, vol. 96, no. 9, pp. 5338-5340, 2004.

[4] S. Islam, M. Faruque, and M. Islam, "The design and analysis of a novel split-H-shaped metamaterial for multi-band microwave applications," *Materials*, vol. 7, no. 7, pp. 4994-5011, 2014.

[5] H. Zhou, C. Wang, and H. Peng, "A novel double-incidence and multi-band left-handed metamaterials composed of double Z-shaped structure," *Journal of Materials Science: Materials in Electronics*, vol. 27, no. 3, pp. 2534-2544, 2016.

[6] H. X. Xu, et al., "Multi-band left-handed metamaterial inspired by tree-shaped fractal geometry," *Photonics and Nanostructures - Fundamentals and Applications*, vol. 11, no. 1, pp. 15-28, 2013.

[7] J. Wang, S. Qu, Y. Yang, H. Ma, X. Wu, and Z. Xu, "Multiband left-handed metamaterials," *Applied Physics Letters*, vol. 95, no. 1, pp. 014105-014105-3, 2009.

[8] X. Jia, X. Wang, Q. Meng, and Z. Zhou, "Tunable multi-band chiral metamaterials based on double-layered asymmetric split ring resonators," *Physica E: Low-dimensional Systems and Nanostructures*, vol. 81, pp. 37-43, 2016.

[9] T. Nesimoglu and C. Sabah, "A tunable metamaterial resonator using varactor diodes to facilitate the design of reconfigurable microwave circuits," *IEEE Transactions on Circuits and Systems II: Express Briefs*, vol. 63, no. 1, pp. 89-93, 2016.

[10] J. Zhao, Q. Cheng, J. Chen, M. Q. Qi, W. X. Jiang, and T. J. Cui, "A tunable metamaterial absorber using varactor diodes," *New Journal of Physics*, vol. 15, no. 4, p. 043049, 2013.

[11] W. Withayachumnankul, C. Fumeaux, and D. Abbott, "Planar array of electric-LC resonators with broadband tunability," *IEEE Antennas & Wireless Propagation Letters*, vol. 10, pp. 577-580, 2011.

[12] B. Zhu, Y. Feng, J. Zhao, C. Huang, and T. Jiang, "Switchable metamaterial reflector/absorber for different polarized electromagnetic waves," *Applied Physics Letters*, vol. 97, no. 5, pp. 051906-051906-3, 2010.

[13] E. Poutrina, "Analysis of nonlinear electromagnetic metamaterials," *New Journal of Physics*, vol. 12, no. 9, 2010.

[14] S. Larouche, A. Rose, E. Poutrina, D. Huang, and D. R. Smith, "Experimental determination of the quadratic nonlinear magnetic susceptibility of a varactor-loaded split ring resonator metamaterial," *Applied Physics Letters*, vol. 97, no. 1, pp. 011109-011109-3, 2010.

[15] D. Huang, E. Poutrina, and D. R. Smith, "Analysis of the power dependent tuning of a varactor-loaded metamaterial at microwave frequencies," *Applied Physics Letters*, vol. 96, no. 10, pp. 104104-104104-3, 2010.

[16] B. Wang, J. Zhou, T. Koschny, and C. M. Soukoulis, "Nonlinear properties of split-ring resonators," *Optics Express*, vol. 16, no. 20, pp. 16058-63, 2008.

[17] A. Velez, J. Bonache, and F. Martín, "Varactor-loaded complementary split ring resonators (VLCSRR) and their application to tunable metamaterial transmission lines," *IEEE Microwave and Wireless Components Letters*, vol. 18, no. 1, pp. 28-30, 2008.

[18] Y. Cheng, Y. Nie, X. Wang, and R. Gong, "Adjustable low frequency and broadband metamaterial absorber based on magnetic rubber plate and cross resonator," *Journal of Applied Physics*, vol. 115, no. 64902, pp. 064902-064902-5, 2014.

[19] Y. Yong-Jun, H. Yong-Jun, W. Guang-Jun, Z. Jing-Ping, S. Hai-Bin, and O. Gordon, "Tunable broadband metamaterial absorber consisting of ferrite slabs and a copper wire," *Chinese Physics B*, vol. 21, no. 3, pp. 504-508, 2012.

[20] Y. Poo, R. X. Wu, G. H. He, and P. Chen, "Experimental verification of a tunable left-handed material by bias magnetic fields," *Applied Physics Letters*, vol. 96, no. 16, pp. 161902-161902-3, 2010.

[21] T. H. Hand and S. A. Cummer, "Frequency tunable electromagnetic metamaterial using ferroelectric loaded split rings," *Journal of Applied Physics*, vol. 103, no. 6, p. 066105, 2008.

[22] D. Shrekenhamer, W.-C. Chen, and W. J. Padilla, "Liquid crystal tunable metamaterial absorber," *Physical Review Letters*, vol. 110, no. 17, p. 177403, 2013.

[23] Q. Zhao, *et al.*, "Electrically tunable negative permeability metamaterials based on nematic liquid crystals," *Applied Physics Letters*, vol. 90, no. 1, p. 011112, 2007.

[24] P. Pitchappa, *et al.*, "Micro-electro-mechanically tunable metamaterial with enhanced electro-optic performance," *Applied Physics Letters*, vol. 104, no. 15, p. 151104, 2014.

[25] C. Sabah, "Tunable metamaterial design composed of triangular split ring resonator and wire strip for

S-and C-microwave bands," *Progress In Electromagnetics Research B*, vol. 22, pp. 341-357, 2010.

[26] J. Wang, *et al.*, "A tunable left-handed metamaterial based on modified broadside-coupled split-ring resonators," *Progress in Electromagnetics Research Letter*, vol. 6, pp. 35-45, 2009.

[27] M. Lapine, D. Powell, M. Gorkunov, I. Shadrivov, R. Marqués, and Y. Kivshar, "Structural tunability in metamaterials," *Applied Physics Letters*, vol. 95, no. 8, p. 084105, 2009.

[28] J. Wang, S. Qu, Z. Xu, and H. Ma, "A controllable magnetic metamaterial: split-ring resonator with rotated inner ring," *IEEE Transactions on Antennas & Propagation*, vol. 56, no. 7, pp. 2018-2022, 2008.

[29] D. Ye, K. Chang, L. Ran, and H. Xin, "Microwave gain medium with negative refractive index," *Nat. Commun.*, vol. 5, p. 5841, 2014.

[30] X. Chen, T. M. Grzegorczyk, B. I. Wu, P. J. Jr, and J. A. Kong, "Robust method to retrieve the constitutive effective parameters of metamaterials," *Physical Review E*, vol. 70, no. 1 pt 2, pp. 811-811, 2004.

[31] J. Zhou, T. Koschny, L. Zhang, and G. Tuttle, "Experimental demonstration of negative index of refraction," *Applied Physics Letters*, vol. 88, no. 22, pp. 221103-221103-3, 2006.

[32] I. Bahl and P. Bhartia, *Microwave Solid State Circuit Design*. Wiley, 2003.

[33] S. Ghosh and A. Chakrabarty, "Estimation of capacitance of different conducting bodies by the method of rectangular subareas," *Journal of Electrostatics*, vol. 66, no. 3-4, pp. 142-146, 2008.

[34] O. Sydoruk, E. Tatartschuk, E. Shamonina, and L. Solymar, "Analytical formulation for the resonant frequency of split rings," *Journal of Applied Physics*, vol. 105, no. 1, pp. 014903-014903-4, 2009.

[35] Available: http://www.skyworksinc.com/uploads/documents/SMV123x_Series_200058W.pdf

[36] A. Sarkhel, D. Mitra, and S. R. B. Chaudhuri, "A compact metamaterial with multi-band negative-index characteristics," *Applied Physics A*, vol. 122, no. 4, pp. 1-10, 2016.